KOGISO, M. & TAKAHASHI, H. (1977). *J. Phys. Soc. Jpn*, **42**, 223–229.
LEHMPFUHL, G. (1972). *Z. Naturforsch. Teil A*, **27**, 425–433.
MARTHINSEN, K., MATSUHATA, H., HØIER, R. & GJØNNES, J. (1988). *Aust. J. Phys.* **41**, 449–459.
MATSUHATA, H. & GJØNNES, J. (1988). *Proc. EUREM* 88, *Inst. Phys. Conf. Ser.* No. 93, Vol. 2, pp. 19–20.
MATSUHATA, H. & STEEDS, J. W. (1987). *Philos. Mag.* **B55**, 17–38.
NIEHRS, H. & WAGNER, E. H. (1955). *Z. Phys.* **143**, 285–299.
REIMER, L. (1989). *Transmission Electron Microscopy*, 2nd ed., p. 286. Berlin: Springer.
SELLAR, J. R., IMESON, D. & HUMPHREYS, C. J. (1980). *Acta Cryst.* A**36**, 686–696.
SHANNON, M. D. & STEEDS, J. W. (1977). *Philos. Mag.* A**36**, 307.
SPELLWARD, P. (1988). *Proc. EUREM* 88, *Inst. Phys. Conf. Ser.* No. 93, Vol. 2, pp. 31–32.
TABBERNOR, M. A., FOX, A. G. & FISHER, R. M. (1990). *Acta Cryst.* A**46**, 165–170.
TAFTØ, J. & GJØNNES, J. (1985). *Ultramicroscopy*. **17**, 329–334.
WATANABE, D., UYEDA, R. & FUKUHARA, A. (1969). *Acta Cryst.* A**25**, 138–140.

Acta Cryst. (1994). A**50**, 115–123

A Study of the Structure Factors in Rutile-Type SnO_2 by High-Energy Electron Diffraction

BY H. MATSUHATA,* J. GJØNNES AND J. TAFTØ

Department of Physics, University of Oslo, PO Box 1048 *Blindern*, 0316 *Oslo, Norway*

(*Received* 29 *March* 1993; *accepted* 12 *July* 1993)

Abstract

The structure factors for low-order reflections of rutile-type SnO_2 have been studied by high-energy electron diffraction. A systematic critical-voltage effect on 220 in 110 systematic reflections, a nonsystematic critical-voltage effect on $1\bar{5}0$ at the [513] zone axis, a nonsystematic critical-voltage effect on the 002 reflection at the [100] zone axis and a [113]-zone-axis critical-voltage effect were observed within the accelerating-voltage range of a 200 kV electron microscope. Analysis of these critical-voltage effects gave experimental values for the structure factors between the theoretical values obtained for the $Sn^{2+}O_2^{1-}$ and $Sn^{4+}O_2^{2-}$ states for low-order reflections like 110 and 011, whereas a structure-factor value between the theoretical values for the neutral SnO_2 and $Sn^{2+}O_2^{1-}$ states was found for the 121 reflection.

1. Introduction

The rearrangement of outer electrons in atoms owing to the bonding in a crystal can be studied by diffraction experiments, in particular at low values of the scattering variable. In this range, electron diffraction will be more sensitive than X-ray diffraction to changes in the atomic scattering factors f^x, as seen from the Mott relation:

$$f^{el}(s) = (me^2/2h^2)[Z - f^x(s)]/s^2,$$

where $s = \sin\theta/\lambda$ and θ, λ, Z, $f^{el}(s)$ and $f^x(s)$ are the scattering angle, electron wavelength, atomic number, electron scattering factors and X-ray scattering factors, respectively; see, for example, Hirsch, Howie, Nicholson, Pashley & Whelan (1965). This advantage is exploited in several electron diffraction methods. Measurement and analysis of the critical-voltage effect (Watanabe, Uyeda & Fukuhara, 1969) caused by the accidental degeneracy of the Bloch wave offer accurate and absolute measurements related to structure factors for low-order reflections, thus providing information on the distribution of outer electrons. Until recently, the critical-voltage effect in the systematic case has been the one mainly utilized. In this case, a high-voltage electron microscope is usually required for the measurement of one or two critical voltages. An extension of the method so that more data for low-order reflections can be obtained and electron microscopes in a more commonly available voltage range can be used appears desirable.

The critical-voltage effect occurs not only in the case of systematic reflections but also in two-dimensional configurations of reflections. Gjønnes & Høier (1971) proposed to extend the method to the nonsystematic case by measuring precise diffraction conditions for the accidental Bloch-wave degeneracy in the Kikuchi pattern. In the preceding paper (Matshuata & Gjønnes, 1994), we presented a development of the nonsystematic critical-voltage method that is applicable in the voltage range of ordinary electron microscopes and that uses the modern convergent-beam technique. Another approach, by

* Present address: Division of Electrodevices, Electrotechnical Laboratory, 1-1-4 Umezono, Tsukuba, Japan.

Shannon & Steeds (1977), is based on the measurement of critical voltages appearing at the exact zone axis. These critical-voltage effects, which are readily observed in the accelerating-voltage range of today's electron microscopes, *i.e.* 100–400 kV, widen the capability for low-angle structure-factor refinement by electron diffraction.

In the present paper, systematic, nonsystematic and zone-axis critical-voltage effects are studied for the refinement of low-order reflections of rutile-type SnO_2. SnO_2 has a tetragonal lattice with space group $P4_2/mnm$ (no. 136). The lattice parameters are $a = 4.736$ and $c = 3.185$ Å. Sn atoms occupy the corner and body-centre positions and O atoms occupy a 4(f) site with position parameter $x = 0.304$ (Bursill, Ping, Smith & Shannon, 1981). The outer electrons of tin, *i.e.* $5s^2$ and $5p^2$, are expected to take part in bonding with two O atoms. The refinement of low-order structure factors by the observation and analysis of the critical-voltage effects is discussed in terms of the effect of ionization in the structure and the localization of bond electrons.

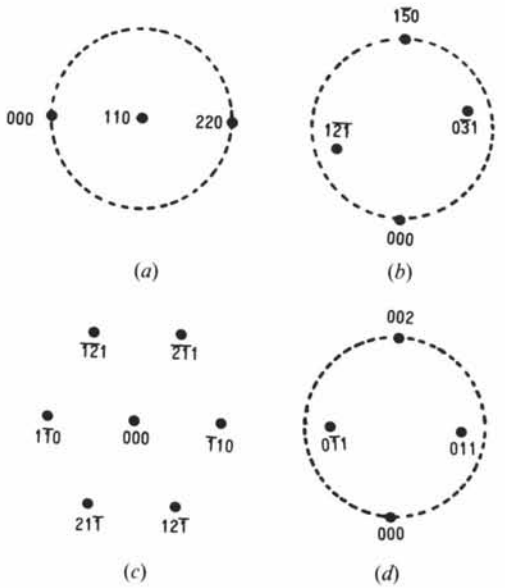

Fig. 1. Diffraction conditions for critical voltages: (*a*) 110 systematic critical voltage; (*b*) nonsystematic critical voltage at the 1$\bar{5}$0 reflection in the [513] zone; (*c*) [113]-zone-axis critical voltage; (*d*) nonsystematic critical voltage at 002 in the [100] zone.

2. Experimental procedure and results

Polycrystalline SnO_2 was made by the isostatic sintering technique. Thin crystals for electron microscopy were prepared by ion thinning, the grain size of several hundred nm being sufficient for the convergent-beam experiment. Transmission electron microscopy was carried out using a JEOL 2000FX in the accelerating range 102 to 203 kV; the accelerating voltage was calibrated by the method proposed by Høier (1969).

The diffraction conditions used for the observations and measurements of the critical-voltage effect are summarized in Fig. 1. Broken circles represent the Laue circles and reciprocal points are indicated by dots. Fig. 1(*a*) represents the 110 systematic critical-voltage effect, observed as extinction at the Bragg position of the 220 reflection. Fig. 2 shows the corresponding large-angle convergent-beam electron diffraction (LACBED) patterns of the direct beam and 220 reflection near the systematic critical voltage of 220. In the bright-field pattern, a characteristic bright contrast at the symmetric position can be seen; in the 220 dark-field pattern, the missing intensity at the exact Bragg position is noted. These observations indicate an accidental degeneracy between Bloch waves 2 and 3. Below the critical voltage, Bloch wave 2 is symmetric and Bloch wave 3 is antisymmetric; above the critical voltage, this sequence is reversed. The critical voltage was measured as 146 (3) kV.

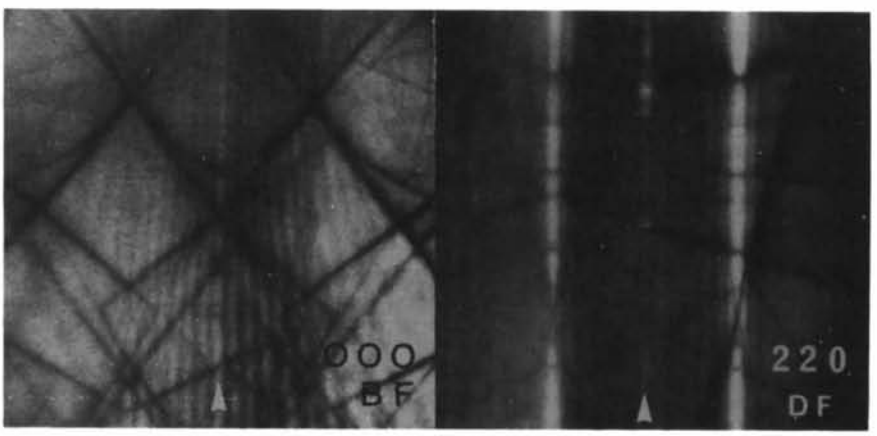

Fig. 2. Large-angle convergent-beam (LACBED) pattern in bright field and 220 dark field taken at 142 kV near the 110 systematic critical voltage. Arrows indicate the symmetric and 220 Bragg positions.

Fig. 1(*b*) illustrates the diffraction condition of an observed skew-diamond type nonsystematic critical-voltage effect on $1\bar{5}0$ at the [513] zone axis, with $1\bar{5}0$ at the Laue circle and $12\bar{1}$ and $0\bar{3}1$ inside the Laue circle. The corresponding convergent-beam patterns are shown in Fig. 3. In Fig. 3(*a*), two points of vanishing contrast are seen in the $1\bar{5}0$ CBED disc, corresponding to a pair of accidental degeneracies of Bloch waves. As the accelerating voltage is increased, these two points move to a position where the projected wave point coincides with the twofold rotation point of the zeroth-order Laue zone. Fig. 3(*b*) is taken near the non-systematic critical voltage which corresponds to this condition: the vanishing contrast is seen in the centre of the $1\bar{5}0$ convergent-beam disc. By further increase of accelerating voltage, the accidental degeneracy disappears, as seen in Fig. 3(*c*). The degeneracy at the critical voltage is between Bloch waves 3 and 4. Below the critical voltage, their symmetries are 2 (symmetric) and 2′ (antisymmetric), respectively; above the critical voltage, the sequence is reversed. Fig. 3(*d*) shows another pair of accidental degeneracies observed in this [513] zone axis at 203 kV in the $\bar{2}13$ reflection. This has the same appearance as the $1\bar{5}0$ reflection at 102 kV and will have a critical voltage above this voltage. The nonsystematic critical voltage for the $1\bar{5}0$ reflection was determined to be 179 (4) kV.

Fig. 4 shows the bright contrast at the exact [113] zone axis in the LACBED pattern, indicating the zone-axis critical-voltage effect. The diffraction condition corresponds to Fig. 1(*c*). At this critical voltage, the sequence of Bloch-wave symmetries of branches 2 and 3 switches from 2*mm* and 2′*m*′*m*, respectively, at a lower voltage, to the opposite order above the critical voltage, which was measured to be 164 (6) kV. This critical-voltage effect can also be regarded as a 110 systematic critical voltage strongly perturbed by four 211 reflections in the zone.

Fig. 1(*d*) shows the diffraction condition for a nonsystematic critical voltage in the 002 reflection near the [100] zone axis, with the 002 reflection at the

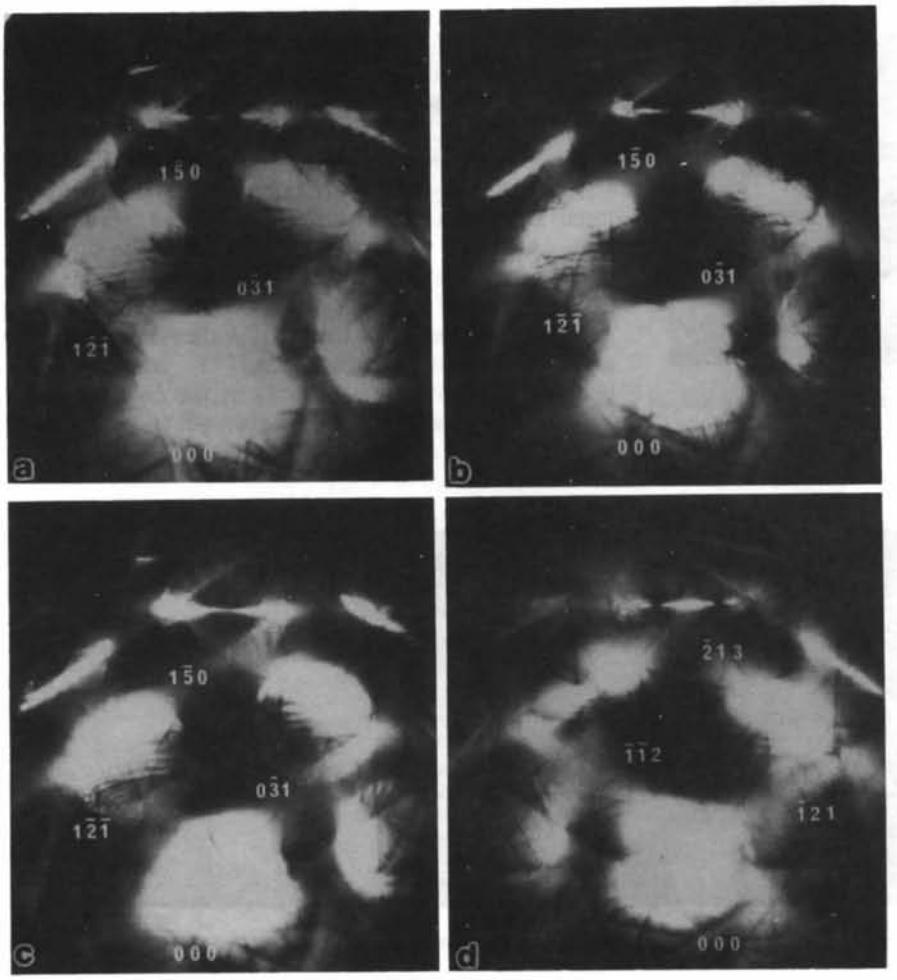

Fig. 3. Patterns showing nonsystematic critical-voltage effects in the [513] zone: (*a*), (*b*) and (*c*) in $1\bar{5}0$; (*d*) in $\bar{2}13$. Patterns taken at (*a*) 102, (*b*) 183 and (*c*) and (*d*) 203 kV.

Laue circle and the $0\bar{1}1$ and 011 reflections inside the circle. Fig. 5 shows the corresponding CBED patterns taken at 102, 153 and 203 kV. Vanishing contrast is observed at 153 kV at the Bragg position in the 002 reflection disc in Fig. 5(*b*). By an increase of accelerating voltage, the $0\bar{1}1$ and 011 discs show reversal of asymmetric contrast owing to the switch of excitation between two Bloch waves. The configuration of the reciprocal points is similar to the previously reported nonsystematic critical voltage seen in 422 in the 111 projection for a face-centred cubic (f.c.c.) structure discussed as a diamond-type nonsystematic critical-voltage-effect (Matsuhata & Gjønnes, 1994). But the shapes of dispersion surfaces and the contrast along the line are rather different, owing to different orders of magnitudes of the structure factors, *viz* $U_{200} > U_{011} > U_{020}$. The position of the vanishing contrast on the 002 line is not sharply defined, with an appearance more like the systematic critical-voltage effect. This nonsystematic critical voltage is estimated to be 153 (7) kV.

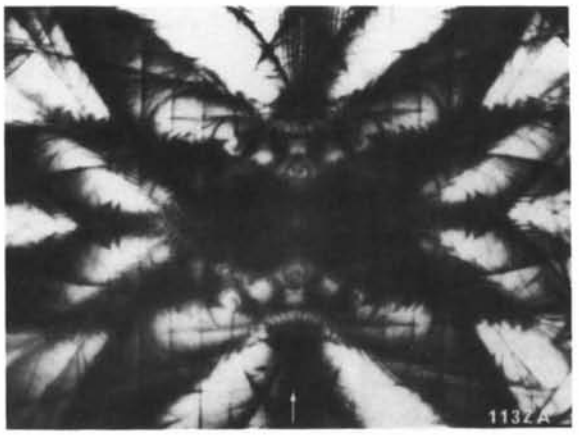

Fig. 4. LACBED patterns at the [113] zone axis near the critical voltage, taken at 183 kV.

3. Analysis of the critical voltages and discussion

(*a*) *Effects of ionization on the scattering factors for low-order reflections*

The four measurements reported above define reflections between several structure factors and will thus depend on a number of structure parameters, including temperature factors as well as charge distribution within the unit cell. The uncertainties associated with higher-order structure factors will be less serious for the inner structure factors, U_{110}, U_{011} and U_{020}, which are particularly sensitive to ionicity. Let us, therefore, start with an interpretation of these in terms of the ionic state of the constituent atoms. Fig. 6 shows the difference between the scattering factors for ionized states and neutral states. The scattering factors are: for Sn, Sn^{2+}, Sn^{4+} and O, functions of scattering angle from Doyle & Turner's (1968) table; for O^{1-}, from Cromer & Mann's (1968) table; for O^{2+}, from Tokonami's (1965) parameter, which he obtained from the band-structure calculation in MgO. Critical voltages were calculated using the scattering factors for the different ionic states with temperature factors obtained by X-ray diffraction (Baur & Kahn, 1971). The number of beams in the dynamical calculations was always above what was found necessary to ensure convergence of the calculated critical voltages. The calculated results are compared with experiments in Table 1; the differences found among various ionization states are generally much larger than the uncertainties in the experimental results, which may indicate at this stage an ionization state between $Sn^{2+}O_2^{1-}$ and $Sn^{4+}O_2^{2-}$ if spherical ions are assumed. In the following, we analyse the measured critical voltages in more detail

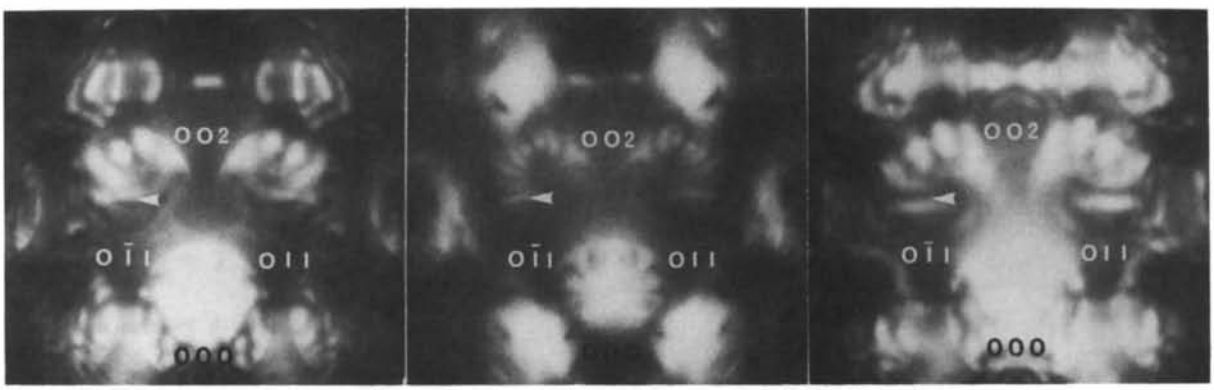

Fig. 5. Nonsystematic critical-voltage effect in the 002 reflection, at the [100] zone axis. From left to right: patterns taken at 102, 153 and 203 kV.

to discuss the structure factors at low-angle reflections.

(*b*) 110 *systematic critical-voltage effect*

In a three-beam approximation, the analytical form of this systematic critical voltage is described as

$$E_c = (m_o c^2/e)\{U_{220}/(U_{110}^2 - U_{220}^2)g_{110}^2 - 1\}. \quad (1)$$

This equation is not sufficient for accurate analysis, but shows the qualitative relations at the systematic critical voltage between U_{110} and U_{220}. If we ignore the temperature factors, the structure factors of the rutile-type crystal are given by

$$F_{hkl} = 2f_{Sn} + 4f_O \cos(2\pi hx)\cos(2\pi kx)$$

for reflections with $h + k + l$ = even and

$$F_{hkl} = -4f_O \sin(2\pi hx)\sin(2\pi kx)$$

for reflections with $h + k + l$ = odd so that

$$F_{110} = 2f_{Sn} + 0.443f_O$$

$$F_{220} = 2f_{Sn} + 2.424f_O.$$

The 110 reflection is seen to depend more on the scattering factor of tin and in particular on its ionicity. The 220 reflection receives a relatively large contribution from the oxygen and appears less sensitive to the ionic state (see also Fig. 6).

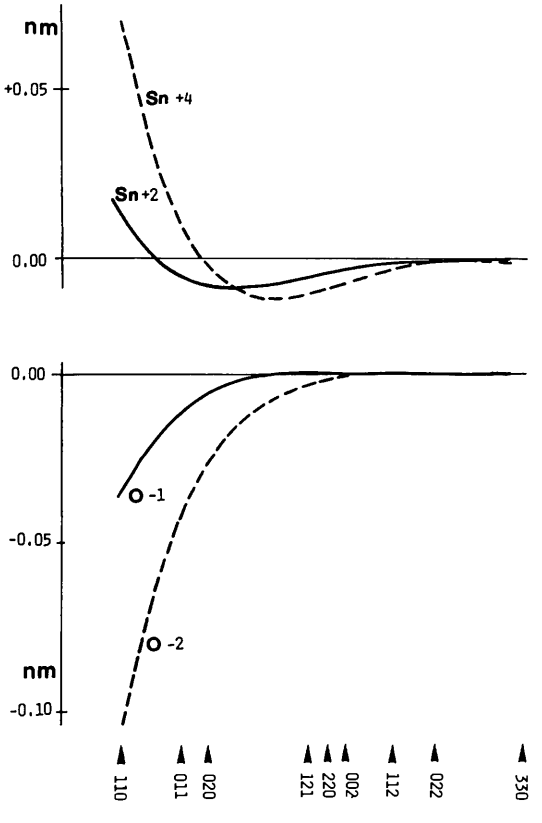

Fig. 6. Calculated electron scattering factors for Sn^{2+}, Sn^{4+}, O^{1-} and O^{2-} plotted as deviations from neutral-atom form factors.

Table 1. *Calculated critical voltages, with scattering factors for different ionic states, compared with experimental values*

	SnO_2	$Sn^{2+}O_2^{1-}$	$Sn^{4+}O_2^{2-}$	Experimental
110 systematic 13-beam calculation	208.7	196.9	73.9	146 (3)
Nonsystematic $1\bar{3}0$ 84-beam calculation	173.2	183.1	207.7	179 (4)
[113] zone axis 99-beam calculation	182.0	181.2	150.4	164 (6)
Nonsystematic 200 198-beam calculation	260.7	250.4	114.2	153 (7)

Scattering factors from Doyle & Turner (1968), Cromer & Mann (1968) and Tokonami (1965); temperature factors from Bauer & Kahn (1971); lattice parameters and atomic positions from Bursill *et al.* (1981). With the lattice parameters and positions of Bauer & Kahn, the calculated critical voltages may shift some kV.

The relationship between U_{110} and U_{220} which satisfies the systematic critical voltage measured experimentally is shown in Fig. 7. The graph was obtained by a 13-beam dynamical calculation, the broken lines indicating the uncertainty from error in the experimental measurement. The different ionic states, *viz* SnO_2, $Sn^{2+}O_2^{1-}$ or $Sn^{4+}O_2^{2-}$, assumed for the other reflections used in these calculations, gave almost the same relation between U_{110} and U_{220}; hence, it is felt that the 110 critical voltage determined experimentally will be almost free from the uncertainties in higher-order reflections arising from ionicity. In Fig. 7 and subsequent figures, the values of U_{110} and U_{220} are given as percentage

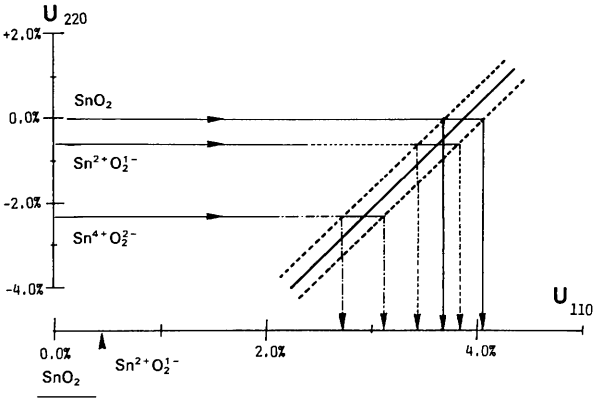

Fig. 7. Analysis of the 110 systematic critical voltage. The relation between the Fourier potentials U_{110} and U_{220} which satisfies the measured critical voltage is represented by the full line. U_{110} and U_{220} are given as precentage deviations from the values obtained from free-atom scattering factors; values for different ionization states are indicated. The broken lines indicate the experimental error range in the measurement. Critical-voltage calculations included 13 beams.

deviations from the free-state SnO_2. It is seen that the assumption of the free-state SnO_2 for U_{220} leads to an increase of 3.85 (20)% in U_{110} compared with the neutral-atom value. Using the $Sn^{2+}O_2^{1-}$ state for U_{220}, we obtained a value for U_{110} that was 3.65 (20)% larger, and with the fully ionized state for U_{220} a value 2.89 (20)% larger than the calculated value for the neutral state for U_{110}. All three models thus lead to a value for U_{110} appreciably larger than that obtained for a neutral state composed of free atoms; *i.e.* they lead to an experimental value corresponding to an ionization state between theoretical Sn^{2+} and Sn^{4+}.

(*c*) *Nonsystematic critical-voltage effect on the* $1\bar{5}0$ *reflection at the* [513] *zone axis*

Using a four-beam approximation, we obtain the eigenvalue

$$2K\gamma(2) = (1/2)\{\beta U_{150} + \beta U_{112} + g^2 - [(\beta U_{150} - \beta U_{112} - g^2)^2 + 4(\beta U_{121} + \beta U_{031})^2]^{1/2}\},$$

for the twofold symmetric Bloch wave and

$$2K\gamma(2') = (1/2)\{-\beta U_{150} - \beta U_{112} + g^2 + [(-\beta U_{150} + \beta U_{112} - g^2)^2 + 4(\beta U_{121} - \beta U_{031})^2]^{1/2}\}$$

for the antisymmetric Bloch wave, 2′, at the twofold position. Here, $g^2 = (g_{112}^2 - g_{150}^2)/4$ and β is the relativistic mass correction.

The nonsystematic critical voltage is obtained when

$$\gamma(2) = \gamma(2'). \qquad (2)$$

It is seen that this critical voltage is sensitive to U_{121} and U_{031} and less sensitive to U_{150} and U_{112}. Ignoring the temperature factors, the structure factors of U_{121} and U_{013} are given by

$$F_{121} = 2f_{Sn} + 1.036f_O$$
$$F_{031} = 2f_{Sn} + 3.404f_O.$$

Of these two structure factors, U_{121} appears more sensitive to the ionic state but, in this range of the scattering variable, the influence of ionicity on the scattering factors is less pronounced than in the low-angle regions. See also Fig. 6; note the change of sign in the curves for the scattering factors of ionized states.

Fig. 8 shows the relation between U_{031} and U_{121} corresponding to the experimentally measured critical voltage, obtained by calculations including 84 beams. Two oblique lines indicate the uncertainty resulting from the experimental error. The effect of different ionic states for higher-indices reflections on the calculations was found to be negligible. Both U_{121} and U_{031} contribute to the critical-voltage effect.

Let us discuss the value for U_{121} in relation to the assumed value of U_{031}. Assuming a U_{031} value corresponding to the free-state SnO_2, we found U_{121} to be smaller than its theoretical value for the state SnO_2 by 0.62 (40)%. The $Sn^{2+}O_2^{1-}$ state for U_{031} led to a 0.65 (40)% smaller value for U_{121} than that for the free state. Both values are seen to be located between the calculated values for the $Sn^{2+}O_2^{1-}$ and SnO_2 states. With the $Sn^{4+}O_2^{2-}$ state assumed for U_{031}, a U_{121} value 0.37 (40)% higher than obtained for the free state was found. If the same ionicity is assumed for U_{031} and U_{121}, a lower degree of ionicity is obtained than was found for U_{011}.

(*d*) [113]-*zone-axis critical-voltage effect*

With a five-beam approximation, an analytical approximation to this critical voltage is given by

$$E_c = (m_o c^2/e)(\{(U_{110} + U_{242})/[2U_{121}^2 - (U_{110} + U_{242}) \times (U_{110} + U_{242} - U_{332})]\}g_{121}^2 - 1). \qquad (3)$$

It is seen from (3) that this critical voltage is sensitive to U_{121}. The graph in Fig. 9, calculated with 99 beams, shows the relation between U_{121} and U_{110} which satisfies the measured value. The value of U_{121} from the assumed U_{110} will be discussed. In this calculation, U_{220} was taken from the experimental relation between U_{110} and U_{220} in Fig. 7. The ranges marked *a*, *b* and *c* along the U_{110} axis in Fig. 9 indicate the U_{110} values obtained from Fig. 7 assuming for U_{220} the free-state SnO_2, $Sn^{2+}O_2^{1-}$, $Sn^{4+}O_2^{2-}$, respectively. The corresponding values for U_{121} are lower than the calculated free-state value by -0.8 (0), -0.7 (10) or -0.4 (10)%, respectively; they vary rather less than the experimental error estimated to 1.0%. The values correspond to an ionic state between neutral and doubly ionized tin, closer

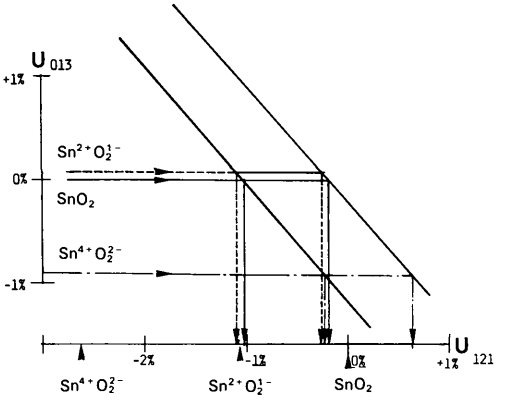

Fig. 8. Analysis of the nonsystematic critical-voltage effect in $1\bar{5}0$. Two full lines represent the measured critical voltages as functions of U_{013} and U_{121}.

to the latter and in fair agreement with the U_{121} value obtained from Fig. 8 with the assumption of ionicity in the same range for U_{013}.

It should be noted that the 110 reflection corresponds to a smaller value of the scattering variable than 121 and 031 and that the slope of the linear relation in Fig. 9 is such that no reliable determination of U_{110} can be obtained from an assumed value of U_{121}. On the other hand, the determination of U_{121} from the critical voltages obtained in the $0\bar{5}1$ reflection and [113] zone axis appears consistent.

(e) Nonsystematic critical-voltage effect on 002 *at the* [100] *zone axis*

Using a four-beam approximation, this critical-voltage effect is given by

$$E_c = (m_o c^2/e)[U_{002}(g_{002}^2 - g_{020}^2)/4 \times (2U_{011}^2 - U_{002}^2 - U_{020}U_{002}) - 1]. \quad (4)$$

This nonsystematic critical-voltage effect depends strongly on the 011 structure factor and somewhat less on 020 and 002. If the temperature factors are ignored, the structure factors of 011, 020 and 002 are given by

$$F_{011} = 2f_{Sn} - 1.331f_O,$$
$$F_{020} = 2f_{Sn} - 3.114f_O,$$
$$F_{002} = 2f_{Sn} - 4.000f_O.$$

These expressions indicate that both U_{110} and U_{020} depend strongly on the ionic state, whereas the 002 structure factor will be much less influenced by ionicity. The ionized effect of tin appears strongly in U_{011}, the effects of both tin and oxygen contributing to U_{020}. The 110 and 020 are both in the low-angle range, *cf.* Fig. 6; hence, this measurement may be expected to be very sensitive to ionicity. This is borne out by Fig. 10, which shows the experimentally determined relation between the two structure factors. The calculations included 198 beams. Different ionic states for outer reflections did not shift the region to a large extent. The small differences in those lines are mainly a result of the different ionic states for U_{002}. An ionic state between Sn^{2+} and Sn^{4+} and close to the latter is found to give the best fit; this agrees well with the value obtained for U_{110} from Fig. 7.

(f) Discussion of the estimated structure factors

The results of the above analysis of the four measured critical voltages can be discussed in terms of two angular ranges; at the low-angle range like 110, 011 and 020, the deviation of scattering factors owing to the ionization is very large and at an intermediate angle range including the 121 and 031 reflections the ionization effect is reduced.

The 220 systematic critical voltage (Fig. 7) and the 002 nonsystematic critical voltage are governed mainly by the inner reflection structure factors U_{110} and U_{011}, and U_{020} The interpretation is not much influenced by ionic states assumed for the outer reflections that entered in the calculations. The value of U_{110} obtained from the analysis is thus considered to be well refined. For U_{011} and U_{020}, only a relation between the two structure factors can be determined from the 002 critical voltage; this relation can be

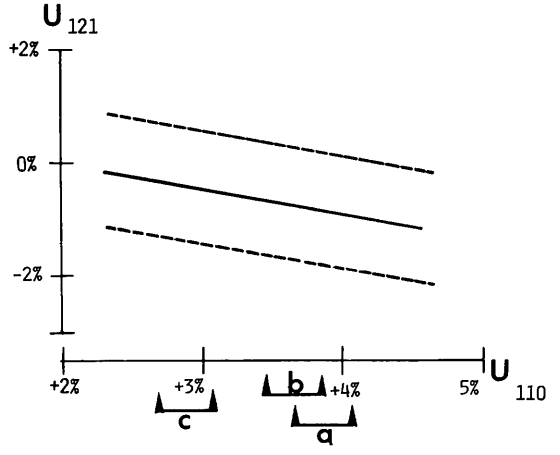

Fig. 9. Analysis of the [113]-zone-axis critical voltage. The parallel lines represent the relation between U_{110} and U_{121}, which corresponds to the measured critical voltage; the broken lines indicate the experimental error. The ranges *a*, *b* and *c* for U_{110} are those obtained from Fig. 7 by assuming U_{220} values corresponding to SnO_2, $Sn^{2+}O_2^{1-}$ and $Sn^{4+}O_2^{2-}$, respectively.

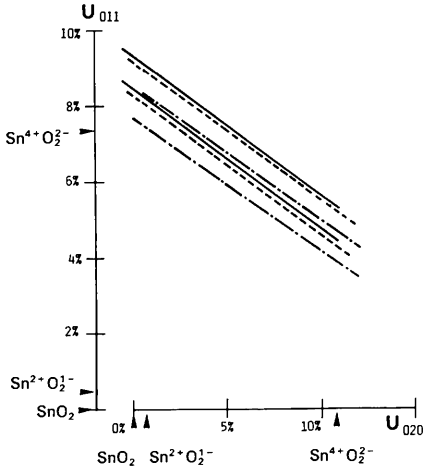

Fig. 10. Analysis of the nonsystematic critical-voltage effect in 002, at the [100] zone: the lines show relations between U_{020} and U_{011} which satisfy the measured critical voltage. The parallel full lines are calculated with neutral atoms assumed for higher-order reflections; broken lines are calculated with $Sn^{2+}O_2^{1-}$; dash–dotted lines with the fully ionized state $Sn^{4+}O_2^{2-}$. The separations of the lines indicate the experimental error.

used together with U_{110} to derive an average ionicity consistent with the inner reflections and assuming spherical ions.

The other two critical voltages, the $1\bar{5}0$ nonsystematic and [113] zone-axis critical voltages, depend mainly on reflections at somewhat higher angles, where the effect of the ionization is much less and the influence of details in the charge distribution may appear. The U_{121} values that were obtained from Figs. 8 and 9 appear consistent; it should be noted that the ionicity which corresponds to this value, assuming spherical ions, fits well with a corresponding value for U_{031} in Fig. 8 and also with a reasonable value for U_{220} in Fig. 7. With these intermediate reflections, we enter a range where bond charges appearing between atoms are expected to be important and the effect of uncertainties in the temperature factor are expected to be more serious. An accurate analysis of these structure factors may thus call for more measurements and extensive treatment, in particular of the temperature effect.

Baur & Kahn (1971) suggested that the rutile-type crystals, TiO_2, GeO_2 and SnO_2 are not completely ionic but have partly covalent bonding. Band structure calculations for SnO_2 by Arlinghaus (1974) indicated a configuration of electrons near the $Sn^{4+}O_2^{2-}$ state but with some contribution from covalent bonding. Recent X-ray and γ-ray studies of TiO_2 indicate the presence of a small hump halfway between the Ti and O atoms in a charge distribution map (Restori, Schwarzenbach & Schneider, 1987). If outer electrons have partly covalent bonding, the effect on the structure factor will depend on the index of the reflections. The ionization effect is expected to appear in the very low angle reflections, as is seen in the present results, where the structure factors for the inner reflections agree well with an ionic state rather close to the configuration $Sn^{4+}O_2^{2-}$.

The results are summarized in Table 2. U_{110} and U_{011} are estimated to be between the theoretical values of the $Sn^{2+}O_2^{1-}$ and $Sn^{4+}O_2^{2-}$ states, rather near the fully ionized state. U_{121} is between the theoretical values of the SnO_2 and $Sn^{2+}O_2^{1-}$ states, and may be more affected by bonding.

The anisotropic temperature factors of Baur & Khan (1971) were used in the present analysis. The experimental errors quoted for these were large and they appear smaller than the temperature factors for other rutile-type crystals. The anisotropic term was found to have little influence on our calculations. If larger temperature factors than the Baur–Kahn values are used, the structure factors will decrease slightly. We have used the lattice parameters and the positioning parameter obtained by Bursill *et al.* (1981). With Baur & Khan's (1971) lattice parameters, the calculated critical voltages will be shifted from a few kV to more than 10 kV, which is of the order of magnitude of experimental uncertainty. The experimentally determined structure factors may be less influenced by an error in the lattice parameter, since the voltage calibration in the experiment will be affected in the same direction.

Table 2. *Experimental and theoretical structure factors, in* 10^{-4} nm^{-2}, *calculated from the critical voltages, with different ionic states assumed for higher-order reflections; theoretical values of structure factors.*

U_{110} experimental
6.896 (13) when SnO_2 is assumed for U_{220}
6.884 (13) when $Sn^{2+}O_2^{1-}$ is assumed for U_{220}
6.833 (13) when $Sn^{4+}O_2^{2-}$ is assumed for U_{220}

U_{110} calculated
6.642 for SnO_2
6.673 for $Sn^{2+}O_2^{1-}$
7.175 for $Sn^{4+}O_2^{2-}$

U_{011} experimental
4.902 when SnO_2 is assumed for higher-order reflections
4.888 when $Sn^{2+}O_2^{1-}$ is assumed for higher-order reflections
4.701 when $Sn^{4+}O_2^{2-}$ is assumed for higher-order reflections

U_{011} calculated
4.504 for SnO_2
4.525 for $Sn^{2+}O_2^{1-}$
4.851 for $Sn^{4+}O_2^{2-}$

U_{121} experimental nonsystematic critical voltage in $1\bar{5}0$
4.273 (17) when SnO_2 is assumed for U_{013}
4.272 (17) when $Sn^{2+}O_2^{1-}$ is assumed for U_{013}
4.311 (17) when $Sn^{4+}O_2^{2-}$ is assumed for U_{013}

U_{121} experimental, [113]-zone-axis critical voltage
4.266 (43) if U_{110} is assumed to be in range *a* of Fig. 9
4.270 (43) if U_{110} is assumed to be in range *b* of Fig. 9
4.283 (43) if U_{110} is assumed to be in range *c* of Fig. 9

U_{121} calculated
4.300 for SnO_2
4.253 for $Sn^{2+}O_2^{1-}$
4.186 for $Sn^{4+}O_2^{2-}$

4. Concluding remarks

The present study shows that the measurement of the critical voltages in the intermediate energy range 100–400 kV can give precise information about the charge distribution in a structure with relatively heavy atoms. The sensitivity to ionicity of the low-angle structure factors is seen to be particularly useful since these are not so sensitive to the uncertainties of other structure factors and thermal parameters and thus may be determined reliably from critical-voltage measurements alone. In particular, for high-atomic-number compounds, the electron diffraction methods appear superior to X-ray methods for studying charge distribution. Except for very simple structures, it is important that several critical voltages are measured.

When the technique is extended to higher values of the scattering variable, the need for combination with other structure information will increase, such as accurate temperature factors and precise values of other structure parameters.

One of us (HM) is grateful to NTNF and NAVF for the financial support. Thanks are due also to Dr T. Norby for help with the specimen preparation.

References

ARLINGHAUS, F. J. (1974). *J. Phys. Chem. Solids*, **35**, 931–935.
BAUR, W. & KHAN, A. (1971). *Acta Cryst.* B**27**, 2133–2139.
BURSILL, L. A., PING, A., SMITH, D. J. & SHANNON, M. D. (1981). *Philos. Mag.* A**45**, 771–789.
CROMER, D. T. & MANN, J. B. (1968). *Acta Cryst.* A**24**, 321–324.
DOYLE, P. A. & TURNER, P. S. (1968). *Acta Cryst.* A**24**, 390–397.
GJØNNES, J. & HØIER, R. (1971). *Acta Cryst.* A**27**, 313–316.
HIRSCH, P. B., HOWIE, A., NICHOLSON, R. B., PASHLEY, D. W. & WHELAN, M. J. (1965). *Electron Microscopy of Thin Crystals.* London: Butterworth.
HØIER, R. (1969). *Acta Cryst.* A**25**, 516–518.
MATSUHATA, H. & GJØNNES, J. (1994). *Acta Cryst.* A**50**, 107–115.
RESTORI, R., SCHWARZENBACH, D. & SCHNEIDER, J. R. (1987). *Acta Cryst.* B**43**, 251–257.
SHANNON M. D. & STEEDS J. W. (1977) *Philos. Mag.* A**36**, 279–307.
TOKONAMI, M. (1965). *Acta Cryst.* **19**, 486.
WATANABE, D., UYEDA, R. & FUKUHARA, A. (1969). *Acta Cryst.* A**25**, 138–140.

SHORT COMMUNICATIONS

Acta Cryst. (1994). A**50**, 123

Multipole analysis of X-ray diffraction data on BeO. Erratum.

By GENEVIÈVE VIDAL-VALAT and JEAN-PIERRE VIDAL, *Groupe de Dynamique des Phases Condensées (UA CNRS* 233), *Université Montpellier* II, 34095 *Montpellier CEDEX* 5, *France*, and KAARLE KURKI-SUONIO and RIITTA KURKI-SUONIO, *Department of Physics, University of Helsinki, Siltavuorenpenger* 20*D*, *PO Box* 9, *SF*-00014 *Helsinki, Finland*

(*Received* 25 *October* 1993)

Abstract

A misprint in the paper by Vidal-Valat, Vidal, Kurki-Suonio & Kurki-Suonio [*Acta Cryst.* (1987), A**43**, 540-550] is corrected.

On Fig. 1, the value 2.7823 Å should read 2.7283 Å.

Professor E.-F. Bertaut is thanked for bringing our attention to this misprint.

Acta Cryst. (1994). A**50**, 123–126

Concerning the components contributing to Bragg reflection profile shapes in synchrotron-radiation studies of small single crystals.

By A. MCL. MATHIESON, *Chemistry Department, La Trobe University, Bundoora, Victoria* 3083, *Australia, and Division of Materials Science and Technology, CSIRO, Private Bag* 33, *Rosebank MDC, Victoria* 3169, *Australia*

(*Received* 22 *July* 1993; *accepted* 8 *September* 1993)

Abstract

Certain basic matters in a recent synchrotron-radiation study [Rossmanith (1993). *Acta Cryst.* A**49**, 80-91] and an allied study which developed a new peak-width formula [Rossmanith (1992). *Acta Cryst.* A**48**, 596-610] are questioned. These matters concern the mode of combination of certain components which determine the one-dimensional profile shape of Bragg reflections and the functional form of the wavelength dispersion dependence on the Bragg angle of the sample crystal and that of a monochromator crystal where the respective crystal axes are parallel.

1. Introduction

A recent synchrotron-radiation study by Rossmanith (1993; hereafter *R*93) dealt with the various individual components which combine to determine the one-dimensional profile shape of Bragg reflections from a small specimen crystal, *c*, as the Bragg angle of the crystal, θ_c, changes. The synchrotron radiation convergent on *c* comes from a monochromator crystal, *M*, and corresponds to a wavelength band, $\Delta\lambda$. In an earlier publication, Rossmanith (1992; hereafter *R*92) introduced an additional component, called the 'particle-size effect' in *R*93, and denoted by ε. By incorporating this component with the wavelength-dispersion component, a new peak-width formula was derived in *R*92 (non-monochromator case) and in *R*93 (monochromator case). The modes of combination of components in *R*92 and *R*93 and the derivation of the functional form of the wavelength dispersion in *R*93 differ significantly from those associated with earlier published works and, therefore, they warrant comment.

2. Identification of the components in diffraction space and their mode(s) of combination (non-monochromator case)

To identify the various components and their contribution to the shapes of one-dimensional profiles, there is considerable advantage in approaching the situation from a two-dimensional